OPEN ACCESS



Correlation of Burst Behavior with Magnetar Age

Özge Keskin 6, Samuel K. Lander, and Ersin Göğüş 6

Faculty of Engineering and Natural Sciences, Sabancı University, İstanbul 34956, Türkiye; ozgekeskin@sabancıuniv.edu

School of Engineering, Mathematics and Physics, University of East Anglia, Norwich, NR4 7TJ, UK

Received 2025 April 15; revised 2025 June 4; accepted 2025 June 5; published 2025 September 8

Abstract

We analyze a wide set of historical magnetar burst observations detected with five different instruments, calibrating these to the energy range of Fermi-GBM observations for consistency. We find a striking correlation between a magnetar's characteristic age and both its typical burst energy and its burst activity level. Arguing that this bursting behavior also correlates with true age, we interpret it as the result of a reducing high-stress volume of the crust in an aging magnetar: Previous giant flares cause relaxation of large regions of its crust and inhibit burst clustering, while the reducing burst energy reflects the progressively shallower region of the crust where Hall drift can build stresses effectively, as the field decays through the range $\sim \! 10^{12} \! - \! 10^{13} \, \mathrm{G}$. Low-energy bursts from very young magnetars may represent failures of weak regions of the crust that have only recently solidified.

Unified Astronomy Thesaurus concepts: High energy astrophysics (739); Neutron stars (1108); Magnetars (992); X-ray bursts (1814)

1. Introduction

One of the most notable and distinctive features of the highly magnetized isolated neutron stars known as magnetars (R. C. Duncan & C. Thompson 1992) is their recurring emission of brief but highly luminous bursts in hard X-rays or soft γ -rays. These bursts, typically lasting ~ 0.1 s, release immense amounts of energy, reaching up to 10^{42} erg (E. Göğüş et al. 2001). Around two-thirds of known magnetars have exhibited such bursts at various occurrence rates (S. A. Olausen & V. M. Kaspi 2014). During a burst-active phase of a magnetar, between a single to thousands of bursts may occur, with activity episodes lasting as long as several months.

Short magnetar bursts are generally attributed to the local yielding of the solid neutron star crust resulting from the release of accumulated elastic stress due to the evolution of the star's internal magnetic field *B* (C. Thompson & R. C. Duncan 1995, 2001). This energy is transferred to the magnetosphere, where a burst may be produced as a result of a magnetic reconnection event, i.e., a rapid untwisting of highly twisted external magnetic field lines (C. Thompson & R. C. Duncan 1995; M. Lyutikov 2003).

In some magnetars, the emission of energetic burst(s) also marks the onset of "magnetar outbursts," enhanced persistent X-ray emission episodes lasting from weeks to years. In their extensive study of X-ray observations of outbursts from 17 magnetars, F. Coti Zelati et al. (2018) showed that the total energy released in each outburst event is inversely correlated with the characteristic age of the star, as determined from its spin period and spin-down rate. In other words, they reported that young magnetars are more likely to exhibit energetic outbursts than older ones. They attributed this behavior to magnetic field decay, which limits the available energy budget as a magnetar ages.

Similarly, when looking at typical short-burst emission, magnetars with low characteristic ages are burst prolific (see,

Original content from this work may be used under the terms of the Creative Commons Attribution 4.0 licence. Any further distribution of this work must maintain attribution to the author(s) and the title of the work, journal citation and DOI.

e.g., A. J. van der Horst et al. 2012; L. Lin et al. 2020b) and often exhibit clusters of bursts (Y. Kaneko et al. 2010, 2021). In this paper, we perform a systematic investigation of short-burst activity behavior in magnetars by utilizing numerous observational studies of magnetar bursts and long-term monitoring of their spin (Section 2), finding an important correlation between burst behavior and age (Section 3), which we show can be used to help understand the evolving stress pattern in a magnetar's crust (Section 4). We then discuss the implications of our study (Section 5).

2. Sample

We aim to characterize typical short bursts emitted by numerous Galactic magnetars over the past three decades. Specifically, we compiled burst fluences from time-integrated spectral studies in the literature. Using distance estimates D for each burst-emitting source, we calculated burst energetics under the assumption of isotropic energy release. Additionally, we gathered the spin period P and its rate of change \dot{P} for each source, allowing us to determine the characteristic ages τ_c of the magnetars in our sample and their inferred dipolar magnetic field strengths (B). We list the compiled database in a table in Appendix A. We also extend the discussion about the distances to sources utilized in this paper in Appendix B.

The compiled burst characteristics are based on analyses of data from five different hard X-ray telescopes. To ensure consistency across all burst properties, we calibrated the fluences by accounting for the sensitivity (detector response) of each telescope. We assume the most characteristic spectral shape of short magnetar bursts, which is a power law (PL) with exponential cutoff whose νF_{ν} spectrum peaks at an energy $E_{\rm peak}$ (L. Lin et al. 2011; A. J. van der Horst et al. 2012). We take model parameters of $E_{\rm peak}=35~{\rm keV}$ and photon index $\Gamma=0$ (A. C. Collazzi et al. 2015; L. Lin et al. 2020a, 2020b). We then obtained conversion factors using Xspec (version 12.14.1) to calibrate fluence values calculated in different energy bands to the energy range of Fermi-GBM observations, since most of the bursts observed in the last two decades were

detected with it. Below, we detail the specific considerations for bursts detected with each of these five instruments.

Fermi-GBM observations. The sample from the Gamma-ray Burst Monitor (GBM) on the Fermi Gamma-ray Space Telescope (Fermi) includes the entire burst observations of SGR 0418+5729, SGR 0501+4516, SGR J1550-5418, Swift J1818.0–1607, Swift J1822.3–1606, 1E 1841–045, PSR J1846.4-0258, SGR J1935+2154, and 1E 2259+586. Moreover, it also includes short bursts of AXP 4U 0142+61 in February 2015 and a single SGR 1806-20 burst in 2010 March. Note that some bright bursts from SGR J1550-5418 (A. J. van der Horst et al. 2012) and SGR 0501+4516 (L. Lin et al. 2011) exceeded the instrumental readout capabilities and caused data saturation. For these cases, we obtained the isotropic burst energies from the nonsaturated time segments of those bright bursts. The fluences (therefore, energies) of Fermi-GBM-detected bursts were reported in the energy range of 8-200 keV.

Swift-BAT observations. Short bursts from AXP 4U 0142 +61 were observed with the Swift Burst Alert Telescope (BAT) in 2011 July and a single burst in 2012 June. Additionally, single bursts from three other sources, SGR J1745–2900, SGR J1833–0832, and Swift J1834.9 -0846, were detected with Swift. Their reported fluences were in the energy range of 15–150 keV. To calibrate these values to 8–200 keV, we obtained a conversion factor of 1.17 by following the approach described earlier. Moreover, the SGR 1900+14 burst forest in 2006 March was detected with Swift. Spectral analysis of the seven slightly longer-duration events during the forest was performed in the energy range of 10–100 keV (G. L. Israel et al. 2008); for these, we assumed an average burst duration of 1 s, and determined a conversion factor of 1.07 to obtain fluence values in 8–200 keV.

CGRO-BATSE observations. For the bursts of SGR 1900 +14 in 1998–1999 and SGR 1806–20 in 1993, 1996, and 1998 observed with the Burst and Transient Source Experiment (BATSE) on board the Compton Gamma Ray Observatory (CGRO), the energy fluences were reported in the energy range of >25 keV; hence, only the minimum energy bound of the integration energy interval is known. Similarly, for the bursts from SGR 1627-41 in 1998, the peak energy flux values were in >25 keV (P. M. Woods et al. 1999). The upper energy bound for fluences (and fluxes) is effectively 200 keV as the spectrum drops exponentially above E_{peak} . We assumed the durations of bursts as 0.1 s, which is the typical burst duration of their sample. Therefore, for the fluences of bursts observed with CGRO (>25 keV), we obtained a conversion factor of 1.59 to calibrate them to 8-200 keV. Finally, we note that, for these observations, the energy fluence/flux ranges of the burst-active episodes (i.e., the minimum and maximum burst fluence/flux values) rather than the individual ones were reported.

INTEGRAL observations. The intense burst-active episode of SGR 1806–20 in 2003–2004 was observed with the International Gamma-Ray Astrophysics Laboratory (INTEGRAL). D. Götz et al. (2006) analyzed the data of 224 bursts during this period in the 15–100 keV range. We estimated the energy fluence range of these bursts by utilizing their fluence histogram; hence, similar to the CGRO-BATSE observations, we have only the burst fluence range instead of having individual fluences. We calculated a

conversion factor of 1.2 for the calibration of fluences in the 15–100 keV band to 8–200 keV.

RXTE-PCA observations. The burst activities from two sources, 1E 1048.1-5937 and XTE J1810-197, presented in this study were observed with the Rossi X-Ray Timing Explorer (RXTE) Proportional Counter Array (PCA). The temporal and spectral analyses of these events were performed in 2-20 keV and 2-30 keV, respectively, for the two sources (F. P. Gavriil et al. 2002, 2006; P. M. Woods et al. 2005). The burst profiles of these sources are quite similar to one another, yet different from those of other sources. As for temporal characteristics, they exhibit longer durations, characterized by a short spike followed by a long tail. Due to its proximity to SGR 1806-20, the identification of XTE J1810–197 as the source of the four bursts observed in 2003–2004 was only possible through the detection of 5.54 s pulsations in the several hundred second-long tails of the events (P. M. Woods et al. 2005). As for spectral characteristics, they have softer spectra that can be modeled with a single blackbody with temperatures around a few keV. That is why the energetics of these events are lower even after applying the integration energy interval calibration.³ We, therefore, keep these bursts out of our sample for further analysis due to their significant spectral and temporal differences, although including or excluding them does not significantly affect our findings. Nevertheless, we still plot them in our figures and note that the reason they have lower yet comparable energetics to regular short and bright magnetar bursts is their long durations due to X-ray-bright tails.

We present magnetar-based burst energies, calibrated as discussed above, versus their calculated characteristic ages in Figure 1. Note again that for the activities observed with CGRO-BATSE and INTEGRAL from the sources SGR 1900 +14 (gold), SGR 1806-20 (green), and SGR 1627-41 (brown), we present burst energy ranges.

3. Results

We observe a relation between the magnetar's burst energy and characteristic age, as seen in Figure 1: Older magnetars emit few bursts with low energies, while younger magnetars exhibit many bursts (often in clusters) with higher energies. To quantify this relation, we fit the trend as follows. We first computed the mean burst energy for each burst-active episode of each source, considering the burst-active episodes/burst clusters separately (see Figure 2). Any cluster size may range from a single burst activity to hundreds of bursts. Our motivation for using burst clusters rather than individual bursts in this analysis was to allow a fairer comparison between sources, rather than deriving a trend heavily skewed by prolific young bursting sources like SGR 1935+2154.

For the burst-active episodes of three sources, observed with CGRO and INTEGRAL, we estimated mean energies by utilizing the reported energy fluence/flux distributions. Guided by the broad trend of the data, as well as theoretical expectations (see the following section), we then fit the mean energy values with a broken power-law (BPL) model (see the solid line in Figure 2). The best fit yields a break $\tau_{\rm break}$ at a characteristic age of 0.9 kyr, with the PL indices before and after the break being 5.40 and -0.54, respectively.

³ We employed a single blackbody model with the reported blackbody temperatures of a few keV, which results in significant emission below 8 keV. Therefore, we calibrated the energies within 2–200 keV instead of 8–200 keV.

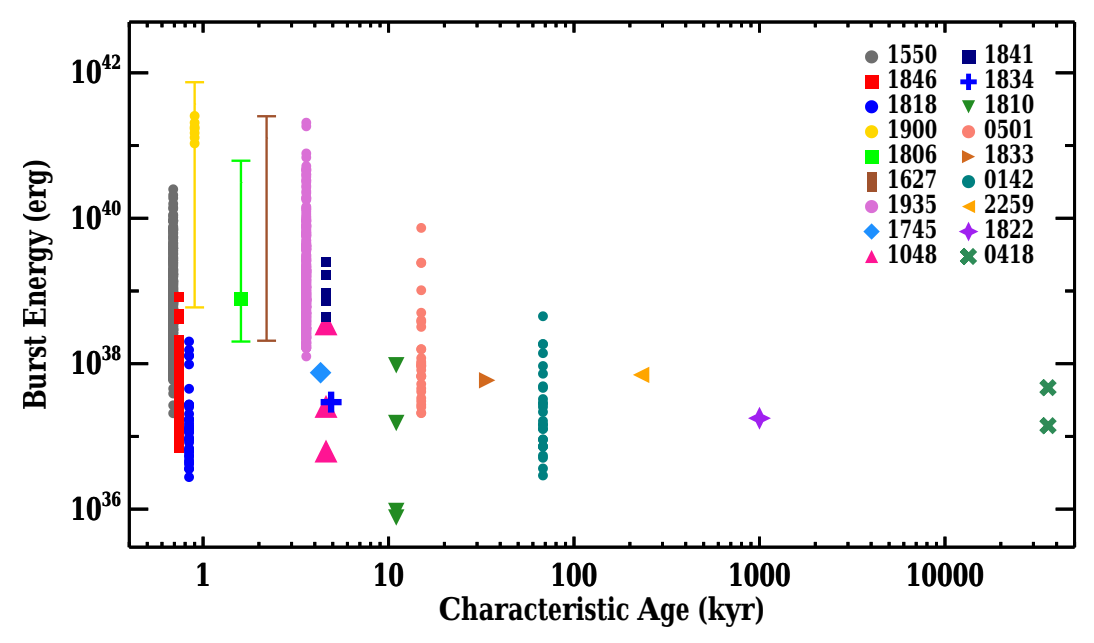


Figure 1. Plot of burst energies vs. characteristic ages of burst-active magnetars. Filled symbols represent the energetics of individual bursts from the color-coded magnetars. For SGR 1900+14 (gold), SGR 1806-20 (green), and SGR 1627-41 (brown), we present burst energy ranges rather than individual burst energies (see text for details). Symbols on the top right are ordered in increasing characteristic age.

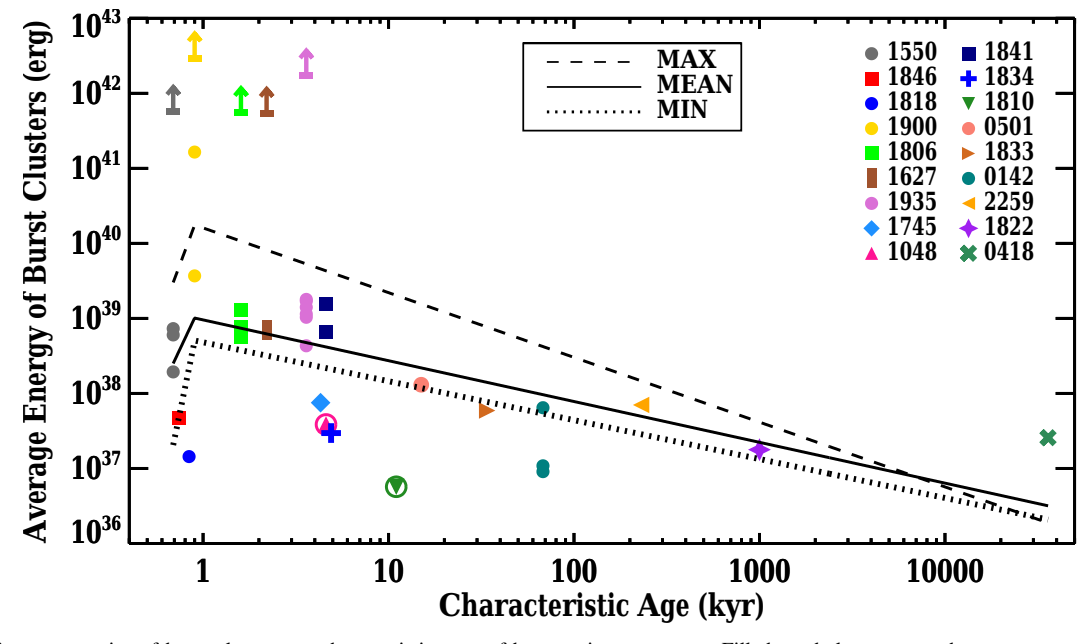


Figure 2. Plot of mean energies of burst clusters vs. characteristic ages of burst-active magnetars. Filled symbols represent the mean energetics of burst-active episodes of the color-coded magnetars. The solid line shown represents the best broken power-law (BPL) fit to the data, with dashed and dotted lines showing BPL fits to the maximum and minimum burst energies of clusters, respectively. The activities of 1E 1048.1–5937 and XTE J1810–197, represented by upward and downward triangles inside circles, were not included in the fits (see the text for details). Upward arrows display the total burst energies considering all activities of the sources in our sample. Symbols on the top right are ordered in increasing characteristic age.

In case of a BPL fit to the minimum energies of each burst cluster (see dotted line in Figure 2), the slopes change to 12.33 and -0.52, respectively, with a break at the same characteristic age. When we fit the maximum burst cluster energies with a BPL (dashed line in Figure 2), we obtain the same break value with indices of 6.62 and -0.88, respectively.

To check possible alternative correlations, we also fitted the minimum, mean, and maximum energies of each burst cluster with a PL model. Finally, we obtained an average burst energy for each source, instead of averaging them per burst cluster, and fitted these data (i.e., minimum, mean, and maximum persource burst energies) to both PL and BPL models.

We list the results of all these fits in Table 1. Fit results are consistent with one another within their 3σ errors. Also, the errors of BPL indices α before τ_{break} are large due to the deficiency of data points before the break (i.e., the few

			BPL		PL
		$ au_{ m break} \ m (kyr)$	α	β	γ
Per burst cluster	Min. Mean Max.	0.90 ± 0.11 0.90 ± 0.19 0.90 ± 0.22	12.33 ± 7.39 5.40 ± 5.95 6.62 ± 9.13	$-0.52 \pm 0.20 \\ -0.54 \pm 0.16 \\ -0.88 \pm 0.25$	$-0.35 \pm 0.19 -0.48 \pm 0.14 -0.78 \pm 0.21$
Per source	Min. Mean Max.	0.96 ± 0.19 0.94 ± 0.38 0.90 ± 0.41	8.90 ± 7.23 4.34 ± 8.18 6.06 ± 15.61	$-0.28 \pm 0.15 -0.37 \pm 0.17 -0.77 \pm 0.33$	$-0.13 \pm 0.14 -0.30 \pm 0.14 -0.69 \pm 0.26$

Note. We show the pre- and postbreak power-law (PL) indices α , β assuming a broken power-law (BPL) model, and the index γ if the data are fitted to a single PL.

magnetars younger than $\tau_{\rm break}$). By contrast, since many data points lie after the breaks of BPLs, the PL indices β for these are better constrained. For the same reason, their values are also compatible with the indices γ of simple PL fits.

4. Theoretical Interpretation

4.1. Physical Differences between Magnetars

Although a number of attributes of a magnetar can be inferred, very few are genuine observables that are common to a number of sources. Our results show a correlation involving three directly observed parameters of burst-active magnetars: their spin period and its time derivative (these two combined into the characteristic age), and their burst activity. Uncertainties in the physics of magnetars allow for various different scenarios to be concocted to explain the observed correlation: In particular, there are very few theoretical constraints on the strength or geometry of a magnetar's magnetic field. Allowing for plausible variations in the external dipole field, the interior toroidal field, and the geometry at the crust—core boundary—together with uncertainties in the material properties of the crust—could potentially allow one to "explain" each of the 16 sources we consider here, while simultaneously not learning anything about them.

In an effort to harness our observed correlation to probe the underlying physics of magnetar bursting, we will adopt an ansatz that the primary physical parameter that governs bursting activity is simply the magnetar's true age. Although this may seem overly restrictive, (i) there is no clear observational evidence that the birth fields of magnetars do vary greatly; (ii) simply because a variety of magnetic field configurations are theoretically permitted, it does not mean they are realized in practice, with, e.g., stability considerations being very restrictive; and (iii) even if a wide range of birth magnetic fields are possible, only a small subset of geometries are likely to lead to magnetar activity (S. K. Lander et al. 2024). As we will see, our ansatz has the virtue of leading to a clear and potentially falsifiable interpretation of the physics driving burst activity—though we cannot, of course, rule out other possible explanations for the burst activity correlation we find.

4.2. True Age of a Magnetar

Figures 1 and 2 show a striking correlation between burst activity and characteristic age. We would like to be able to take the latter quantity as a proxy for *true* age, which would then allow us to draw valuable insights into the evolution of magnetars from these figures. Let us, then, consider how well characteristic and true age are likely to be correlated.

The characteristic age gives a timescale for the present-day spin-down of a neutron star, but magnetars can experience substantial spin-down variation on short timescales due to their coronal twists (C. Thompson & R. C. Duncan 2001; C. Thompson et al. 2002; A. M. Beloborodov & C. Thompson 2007). A recent example of this is SGR 1818.0–1607, discovered during a period of outburst and described as "very young" with its initially reported $\tau_c=240\,\mathrm{yr}$; but 2 yr later its spin-down had stabilized, resulting in a revised (and more typical) $\tau_c=840\,\mathrm{yr}$ —nearly 4 times the earlier value. The danger of such misleading τ_c can thus be somewhat ameliorated by avoiding epochs around significant outbursts/bursting activity, and we have done so in the values we report here.

A more striking example of this is SGR 1806-20, which showed long-term variability in its spin-down rate between 2000 and 2011, with its spin frequency derivative $(\dot{\nu})$ increasing an order of magnitude following its giant flare on 2004 December 27 (P. M. Woods et al. 2007; G. Younes et al. 2015). The characteristic age of the source was reported as 0.24 kyr using P and \dot{P} values measured in this active phase (S. A. Olausen & V. M. Kaspi 2014), whereas G. Younes et al. (2017) calculated a characteristic age of 1.6 kyr based on observations with NuSTAR after 11 yr following the giant flare, and found that $\dot{\nu}$ had stabilized to its historical minimum value measured in 1996 by P. M. Woods et al. (2000). However, during the long active phase of the source, its spin period decreased by 3%, far more significantly than what is expected from the nominal value. Accumulation of this magnitude over several kiloyears could lead to large discrepancies between the characteristic and true age of the magnetar.

It is occasionally possible to estimate magnetar ages from proper-motion measurements and associations with star clusters; S. P. Tendulkar et al. (2012) used this method to estimate the true ages of SGRs 1806-20 and 1900+14 as being, respectively, 0.65 ± 0.30 kyr and 6.0 ± 1.8 kyr—results reasonably consistent (within a factor of 5) with the τ_c we report here. Note that this age-estimation method has its own inherent uncertainties, too. Another possible way to estimate the true age of a magnetar is the calculation of the associated supernova remnant (SNR) age, if any. As an example, PSR 1846.4-0258 is located in the young SNR Kesteven 75, whose age is consistent with the characteristic age of the pulsar (E. V. Gotthelf et al. 2000; M. A. Livingstone et al. 2011; D. A. Leahy & W. W. Tian 2008a). On the other hand, 1E 2259+586, with a spin-down age of \sim 230 kyr, may have a true age of ~ 10 kyr, given its location near the center of the X-ray-bright SNR CTB 109 (M. Sasaki et al. 2004, 2013; M. Sánchez-Cruces et al. 2018). This implies that, even at this

young age, the evolution can deviate significantly from that of an assumed magnetic dipole (with braking index n=3). The greatest deviations of τ_c from true age can be expected from sources with $\tau \gtrsim 100$ kyr, where evolution of the star's crustal field and rotation mean the long-term average spin-down is likely to have been very different from that seen in present-day observations. For example, SGR 0418+5729 has $\tau_c \sim 36,000$ kyr, but a true age estimated as ~ 550 kyr from a magnetothermal evolution (N. Rea et al. 2013), and just 18 kyr from a study modeling its magnetospheric evolution (T. Mondal 2021).

Another argument in favor of using Figures 1 and 2 to infer a correlation between burst energy and true age is that there is no obvious physical reason for burst energy to be correlated with τ_c per se; bursts are believed to be powered by crustal stresses rather than the star's spin-down. By contrast, there is a good reason to expect burst energy to reduce with true age, as magnetic field decay results in a significant reduction in magnetic energy over a timescale of $\sim 10 \, \mathrm{kyr}$ (see, e.g., J. A. Pons & U. Geppert 2007; C. Dehman et al. 2023), consistent with Figure 1. We explore this in the following subsections, where we argue that the bursting behavior of a magnetar gives us insights into the size of highly stressed regions in the star's crust and how these change over time.

4.3. Aging Magnetars: The Effect of Ohmic Decay

The interplay between Hall drift and ohmic decay causes the evolution and decay of the crustal magnetic field. To understand this process, we begin by defining the characteristic timescales for these effects:

$$\tau_{\text{Ohm}} = \frac{4\pi\sigma L^2}{c^2}, \quad \tau_{\text{Hall}} = \frac{4\pi\rho_e L^2}{cR}, \tag{1}$$

where σ is the electrical conductivity, ρ_e the charge density, and L a characteristic length scale for the magnetic field. We may then approximate the resulting field decay with the formula (D. N. Aguilera et al. 2008)

$$B(t) = B_0 \frac{\exp(-t/\tau_{\text{Ohm}})}{1 + \frac{\tau_{\text{Ohm}}}{\tau_{\text{Hall}}} (1 - \exp(-t/\tau_{\text{Ohm}}))},$$
 (2)

where B_0 is the initial field (note that during the phase that interests us, B(t) is insensitive to any choice of B_0 greater than $\sim 10^{14}$ G, as shown later). From these timescales, we can also define the *Hall parameter*:

$$R_{\rm H} \equiv \frac{\tau_{\rm Ohm}}{\tau_{\rm Hall}} = \frac{\sigma B}{c \rho_e},\tag{3}$$

where $R_{\rm H}$ defines the dominant field-evolution mechanism: $R_{\rm H} > 1$ for Hall drift, $R_{\rm H} < 1$ for ohmic decay.

Let us first consider the population of magnetars with $\tau_c \gtrsim 5$ kyr. Their observed reduction in burst energy cannot simply be that ohmic decay causes a slowing in stress buildup from Hall drift. Were that the case, then—in the absence of other changes to the crust—we would expect to observe bursts of the same size but reduced frequency as the star ages. Although some evolution of the material properties of the crust is expected—for example, the yield stress does have some dependence on temperature and strain rate (A. I. Chugunov & C. J. Horowitz 2010), direction (D. A. Baiko & A. A. Kozhberov 2017), and crystalline structure (D. A. Baiko &

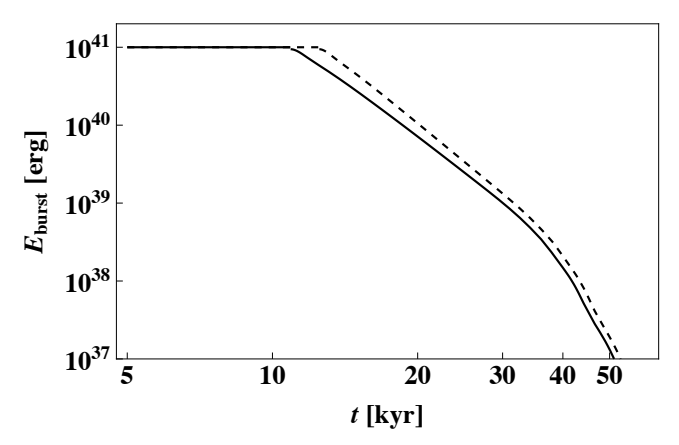


Figure 3. The reduction in elastic energy storage, due to an encroaching region where ohmic decay dominates (see text for details), causes the predicted burst energy $E_{\rm burst}$ to decrease as a function of true age t of a magnetar. Solid and dashed lines show the evolution of models with initial magnetic field strengths of 10^{14} G and 5×10^{15} G, respectively.

A. I. Chugunov 2018)—these factors alone are unlikely to account for the observed correlation between burst energies and stellar age.

Instead, let us look at the depth of the crustal region where Hall drift is faster than ohmic decay (i.e., where $R_{\rm H} > 1$), considering a density ρ range from $10^{10}\,\mathrm{g\,cm^{-3}}$ at the top of the crust (a typical choice, avoiding the lowest-density half of the outer crust, which may not even be solid) to $1.4 \times 10^{14} \,\mathrm{g \, cm^{-3}}$ at the base, where the crust meets the core. Only when $R_{\rm H} > 1$ do we expect crustal stresses to develop. For young magnetars, with typical field strengths $B \gtrsim 10^{14}$ G, the whole crust is in a Hall-dominated state. For a spatially constant crustal B, the first region that switches from Hall to ohmic dominated is the base. As a specific example, using the same profiles for ρ , ρ_e , and σ as in K. N. Gourgouliatos & S. K. Lander (2021), this occurs when $B = 1.2 \times 10^{13} \,\mathrm{G}$. At progressively lower field strengths, the $R_{\rm H} < 1$ region spreads, leaving an increasingly shallow Halldominated layer. Finally, the "top" of the crust reaches $R_{\rm H} = 1$ when B drops to 2.1×10^{12} G. As a result, for a reducing field strength, the maximum elastic energy that can be generated within the crust due to Hall drift also reduces, and when $B \lesssim 2.1 \times 10^{12}$ G, no "new" stress can be generated anywhere. (Old stresses could, of course, remain from an earlier epoch of Hall drift, unless these have been reduced by previous seismic activity or other effects.)

As an illustrative toy model, let us assume that when the entire crust is in a Hall-dominated phase, the largest possible individual short burst is $10^{41}\,\mathrm{erg}$, corresponding to a fixed fraction 1.2×10^{-6} of the star's maximum possible elastic energy E_{max} , i.e., the energy that would be stored if the entire crust were at its yield stress. In the gradually reducing Hall-dominated volume of the crust that results from field decay, the total elastic energy reduces to some fraction of E_{max} , and the predicted maximum burst energy decreases in the same way. If we now combine this with the prescription for field decay in Equation (2), we can calculate a predicted burst energy as a function of stellar age, which we plot in Figure 3.

4.4. Very Young Magnetars

The brightest short bursts come from sources with τ_c in the range 0.9–3.6 kyr. Given the uncertainty in how this relates to true age (see Section 4.2), these magnetars might very well all

be the same age. Before this broad peak, there are three "young" magnetars, each with a very similar τ_c value (all <0.9 kyr), and each having emitted a large number of relatively weak bursts. Although the weakness of their bursts alone is also consistent with these magnetars being far older than their τ_c values, the profusion of the bursts indicates that they are indeed young.

Large numbers of weak bursts are consistent with the way stresses are likely to develop in a young magnetar. A magnetar's crust freezes only gradually, from the inside out, and its yield stress is considerably lower when it has just solidified (A. I. Chugunov & C. J. Horowitz 2010). Below a true age of \sim 1 kyr, Hall drift will not have had time to bring a large portion of the crust to its zero-temperature yield stress, but frequent failures of its weak, hot, outer crust are plausible. While we should be circumspect about Figure 2's apparent positive correlation between burst energy and age for very young ($\tau_c \lesssim 1 \, \text{kyr}$) magnetars, given that it is based on a limited number of sources with poorly constrained true age, there is a physical reason to expect such a correlation: Progressively deeper failures, releasing more energy, become possible only as the star ages, and its crust cools further and becomes more stressed.

4.5. Size of Burst Clusters

In addition to the correlation between burst energy and τ_c , Figure 1 also shows a notable reduction in the total number of bursts a magnetar is likely to emit as it ages. One might worry that this result could be heavily affected by how long we have been observing a given magnetar, but in fact magnetars tend to have rare very active episodes (often when they are discovered)-where many bursts are emitted in a clusterand long periods of quiescence. For example, although the first bursts from SGR 1806-20 were seen in 1979 (B. Cheng et al. 1996) and it has been monitored since then, no intense bursting episode has been observed from this source in the last two decades (D. Götz et al. 2006). As before, considering the attributes of individual burst clusters allows for a fairer comparison between sources, and the number of bursts in a cluster is seen to decrease with τ_c . Again, taking this as a proxy for true age, it appears that the physical size of active regions on a magnetar decreases notably as it ages.

Building on our earlier paper (Ö. Keskin et al. 2024), where we modeled burst clusters as being due to interactions between local highly stressed cells of the crust and their neighboring cells, we are also able to interpret the decrease in burst cluster size with age. In the crust of a young magnetar (the focus of our previous paper), large regions are at a stress close to the elastic yield value, beyond which failure—together with the release of some elastic energy-must occur. When any given cell fails, therefore, it is likely to trigger the successive failure of several neighbors, thus producing a cluster of bursts. An older magnetar, however, may have suffered a number of large events—such as giant flares—over its seismic history, leaving low stress levels in a large volume of the crust. Such extensive failures were excluded from the modeling in Ö. Keskin et al. (2024), which was concerned with short-timescale phenomena, but can trivially be reenabled in the code, using the original deep-failure prescription from S. K. Lander (2023). To understand how burst clustering may change over time, we compare the burst number distribution per cell over 1 kyr of evolution for two scenarios: one young magnetar—assumed to

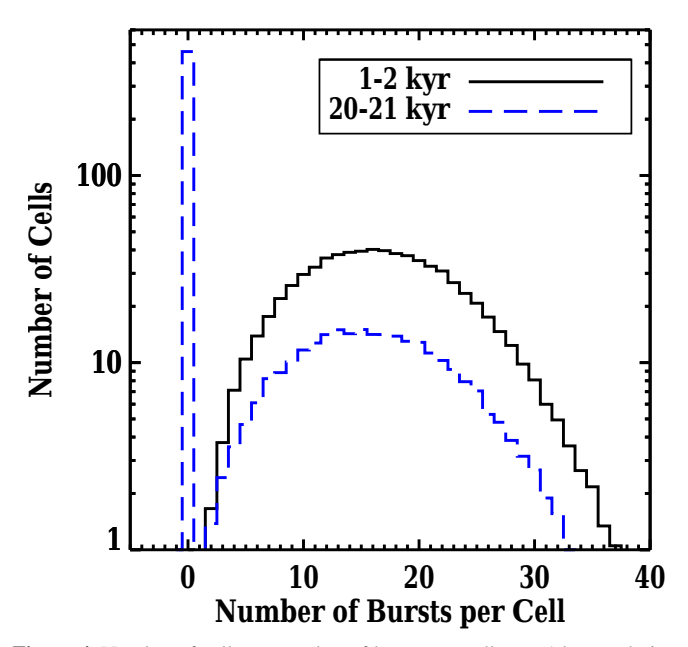


Figure 4. Number of cells vs. number of bursts per cell over 1 kyr evolution. The black solid line displays the burst number distribution per cell, obtained as an average of 100 simulations, for a young magnetar whose age is between 1 and 2 kyr. The blue dashed line represents the same relation for an older (20–21 kyr) magnetar. The accumulation of cells giving zero bursts corresponds to cells that have previously suffered deep failures and are therefore currently experiencing no remaining stress.

become burst active at an age of 1 kyr and not to suffer any deep failures over the following kiloyear—and one old magnetar that has already evolved over a 20 kyr period that included deep failures. The two distributions are compared in Figure 4. It is clearly seen that cells in the older magnetar are less active, with many being completely inactive (see the accumulation of cells giving zero bursts in the figure) due to having no remaining stress. As a result, the failure of a cell in an aging magnetar will typically trigger failure in far fewer neighbors, thus reducing the size of burst clusters.

5. Discussion

The suggestion of a correlation between burst activity and magnetar age is not new: R. Perna & J. A. Pons (2011) found a way to account for this in their pioneering study on the link between crustal failure and magnetic field evolution. What we offer here is a quantitative study of the correlation based on decades of burst data, carefully treated in a way that permits direct comparison. Comparing very young, typical, and aging magnetars, we show how their burst activity helps build a more quantitative picture of how, where, and when crustal stresses develop and are relieved. This complements our earlier work on the burst activity of typical magnetars (Ö. Keskin et al. 2024), and on the full range of crust-driven energy output from magnetars (S. K. Lander 2023).

With clear expectations both from observations and theory, our work provides a method to estimate the age of a magnetar based on its burst activity alone and to construct a complete history of a magnetar's crust. The crust solidifies gradually, from the inside outwards, over a period of centuries. At the point of freezing, it must be in an unstressed state, since a fluid cannot resist shear stresses. This early phase of crustal evolution, taking perhaps ~ 1 kyr, is complex: As well as undergoing magnetothermal evolution, coupled with plastic

flow, the crust itself is changing in both thickness and its mechanical properties. No simulation to date has addressed this in a self-consistent manner. However, given the newborn crust's limited ability to develop and release significant stress, we predict that no "conventional" magnetar activity, i.e., powered by crustal stresses, will be detectable from a star with age $\lesssim 0.5$ kyr.

As a magnetar approaches an age of ~ 1 kyr, crustal failures have the potential to become progressively deeper and to release more energy. The number of bursts in a typical cluster is large; any local failure is likely to trigger neighboring failures. Magnetars in the age range $\sim 1-10$ kyr are likely to display fairly similar burst activity, both in energy and number. This is, however, also the phase where very rare giant flares are most likely to occur, releasing huge amounts of energy and destressing large volumes of the crust (S. K. Lander 2023).

When the low-stress regions have grown sufficiently in volume, the magnetar's ability to produce large burst clusters becomes compromised. Furthermore, new stresses can develop only within a diminishing thickness of the crust, reducing the average burst energy. This phase, for an age $\sim\!10\text{--}100\,\mathrm{kyr},$ ends with the magnetar becoming silent.

In this study, we chose to analyze the correlation of magnetar burst activity with characteristic age, as calculated from the observed spin-down parameters P and \dot{P} . We could instead have compared burst activity with inferred dipole field strength, which is also derived from spin-down parameters and is slightly less sensitive to fluctuations in \dot{P} . It is, however, a more indirect proxy for the age of the source. A plot showing the correlation of burst activity with inferred dipole field strength is given in Appendix C.

The scenario we propose in this paper is, of course, based on qualitative results about field evolution rather than the detailed 3D magnetothermal evolutions of the problem that are now available, which couple both the magnetic field and thermal evolution of the crust, with realistic microphysical parameters (e.g., D. De Grandis et al. 2021; A. P. Igoshev et al. 2021; S. Ascenzi et al. 2024). What these studies miss, however, is a realistic treatment of crustal failure, and so can only be taken as truly quantitative when the crust is below its yield stress. Furthermore, the initial field and the crust-core boundary condition used in simulations can lead to serious variations in the evolution and predicted burst activity (C. Dehman et al. 2023; S. K. Lander et al. 2024). These uncertainties provide a rationale for more qualitative work like ours, focusing on interpreting observations through models of the buildup and release of stress, with the intention that this can guide more realistic treatments of crustal evolution at high stress in the future.

Acknowledgments

This work was supported by a Royal Society International Exchange grant No. IES\R3\223220 between the University of East Anglia and Sabancı University.

Appendix A The Sample

We list our sample in Table 2. The list includes the name of the sources, their spin periods (P) and period derivatives (\dot{P}) , inferred dipolar magnetic field strengths (B) and characteristic ages (τ_c) by using $P-\dot{P}$, as well as their distance estimates (D) and the energy ranges of their emitted short bursts, together with all their corresponding references.

 Table 2

 List of Burst-active Magnetars and Their Characteristics

Source Name	<i>P</i> (s)	$(10^{-11} \text{ s s}^{-1})$	$ au_c^{ m a}$ (kyr)	(10^{14} G)	D (kpc)	Burst Energy ^c (10 ³⁸ erg)	References ^d
AXP 4U 0142+61	8.69	0.20	68	1.34	3.6	[0.03, 4.5]	(1), (2), (3)
SGR 0418+5729	9.08	0.0004	~36,000	0.06	2	[0.14, 0.47]	(4), (5), (6)
SGR 0501+4516	5.76	0.594	15	1.87	2	[0.21, 73.72]	(7), (8), (9)
1E 1048.1-5937	6.46	2.22	4.6	3.83	9	[0.06, 3.53] ^e	(1), (2), (10), (11)
SGR J1550-5418	2.07	4.77	0.69	3.18	5	[0.21, 250.56]	(12), (13), (6)
SGR 1627-41	2.59	1.90	2.2	2.24	11	[2.07, 2532.66]	(14), (15), (16), (17)
SGR J1745-2900	3.76	1.39	4.3	2.31	8.3	0.75	(18), (19), (20)
SGR 1806-20	7.75	7.51	1.6	7.72	8.7	[2.02, 619.31]	(21), (22), (23), (24), (6)
XTE J1810-197	5.54	0.78	11	2.10	3.5	[0.008, 0.95] ^e	(25), (26), (27)
Swift J1818.0-1607	1.36	2.55	0.84	1.88	4.8	[0.03, 2.02]	(28), (29), (30)
Swift J1822.3-1606	8.44	0.013	~1000	0.34	1.6	0.18	(31), (32), (6)
SGR J1833-0832	7.57	0.35	34	1.65	5.7	0.59	(33), (20), (34)
Swift J1834.9-0846	2.48	0.796	4.9	1.42	4.2	0.30	(35), (36), (37)
1E 1841-045	11.78	4.08	4.6	7.02	8.5	[4.41, 25.07]	(1), (38), (6)
PSR J1846.4-0258	0.33	0.71	0.74	0.49	6	[0.07, 8.16]	(39), (40), (30)
SGR J1900+14	5.20	9.20	0.9	7.00	12.5	[5.95, 7432.91]	(41), (42), (43), (44)
SGR J1935+2154	3.24	1.43	3.6	2.18	9	[1.26, 2065.91]	(45), (46), (47)
1E 2259+586	6.98	0.048	~230	0.59	3.2	0.70	(1), (48), (6)

Notes.

References. (1) R. Dib & V. M. Kaspi (2014); (2) M. Durant & M. H. van Kerkwijk (2006); (3) E. Göğüş et al. (2017); (4) N. Rea et al. (2013); (5) A. J. van der Horst et al. (2010); (6) A. C. Collazzi et al. (2015); (7) A. Camero et al. (2014); (8) Y. Xu et al. (2006); (9) L. Lin et al. (2011); (10) F. P. Gavriil et al. (2002); (11) F. P. Gavriil et al. (2006); (12) R. Dib et al. (2012); (13) A. Tiengo et al. (2010); (14) P. Esposito et al. (2009b); (15) P. Esposito et al. (2009a); (16) S. Corbel et al. (1999); (17) P. M. Woods et al. (1999); (18) V. M. Kaspi et al. (2014); (19) G. C. Bower et al. (2014); (20) J. A. Kennea et al. (2013); (21) G. Younes et al. (2017); (22) J. L. Bibby et al. (2008); (23) E. Göğüş et al. (2000); (24) D. Götz et al. (2006); (25) F. Camilo et al. (2007); (26) A. H. Minter et al. (2008); (27) P. M. Woods et al. (2005); (28) K. M. Rajwade et al. (2022); (29) M. E. Lower et al. (2020); (30) M. Uzuner et al. (2023); (31) G. A. Rodríguez Castillo et al. (2016); (32) P. Scholz et al. (2012); (33) P. Esposito et al. (2011); (34) E. Göğüş et al. (2010); (35) O. Kargaltsev et al. (2012); (36) D. A. Leahy & W. W. Tian (2008b); (37) V. D'Elia et al. (2011); (38) W. W. Tian & D. A. Leahy (2008); (39) M. A. Livingstone et al. (2011); (40) D. A. Leahy & W. W. Tian (2008a); (41) S. Mereghetti et al. (2006); (42) B. Davies et al. (2009); (43) E. Göğüş et al. (1999); (44) G. L. Israel et al. (2008); (45) G. L. Israel et al. (2016); (46) L. Lin et al. (2020a); (47) L. Lin et al. (2020b); (48) R. Kothes & T. Foster (2012).

Appendix B Distances

To calculate the burst energetics of the sources in our sample, we utilized the distances to the sources provided and commonly accepted in the literature. Many of the sources in our sample were assigned to a distance with large uncertainties by associating them with a region, a nearby system, a star cluster, or a SNR. These uncertainties may stem from measurement/method errors or approximate estimations.

As examples of magnetars that are associated with a region, SGR 0418+5729 and SGR J0501+4516 both lie on the Galactic plane and in the direction of the Galactic anticenter (A. J. van der Horst et al. 2010). Since many stars in that direction reside in the Perseus spiral arm of the Milky Way,

and the distance to the arm was determined to be 1.95 ± 0.04 kpc by Y. Xu et al. (2006), the distance to both magnetars was commonly accepted as ~ 2 kpc in the literature. SGR J1745-2900 serves as an example of a source whose distance is obtained due to its proximity to a known system: It sits near the Galactic center (Sagittarius A*), which is located at a distance of 8.3 ± 0.3 kpc from the Sun (G. C. Bower et al. 2014). Similarly, SGR J1833-0832 is assumed to be at a distance of 5.67 kpc, based on a likely association with the nearby star-forming region containing PSR J1830-08, which is roughly 3'.7 away from the magnetar (E. Göğüş et al. 2010).

One alternative way of calculating distances is using spectroscopy for the associated host clusters that contain magnetars. J. L. Bibby et al. (2008) and B. Davies et al. (2009)

^a Characteristic age, $\tau_c = P/2\dot{P}$.

b Inferred dipolar magnetic field strength, $B = (3c^3IP\dot{P}/8\pi^2R^6)^{1/2} = 3.2 \times 10^{19}(P\dot{P})^{1/2}$ assuming I = 45 g cm² and R = 10 km.

^c In 8–200 keV.

^d Numbers given in parentheses correspond to the references of $P \& \dot{P}$, distance (D), and burst energetics for each source, respectively.

^e In 2–200 keV.

used this technique and obtained the distances to the magnetars SGRs 1806–20 and 1900+14 and their associated clusters as $8.7^{+1.8}_{-1.5}$ kpc and 12.5 ± 0.3 kpc, respectively. Magnetar–SNR associations provide another alternative way for distance measurements. For example, SGR J1550-5418 is associated with the radio shell G327.24-0.13. By associating these with SNRs G326.96+0.03 and G327.99-0.09 that reside within the distance range of 3.7-4.3 kpc, J. D. Gelfand & B. M. Gaensler (2007) proposed a distance of \sim 4 kpc to SGR J1550–5418. Using the observations of the X-ray rings centered on the same magnetar following the burst storm observed on 2009 January 22, A. Tiengo et al. (2010) measured the distance as \sim 4–5 kpc, consistent with J. D. Gelfand & B. M. Gaensler (2007). 1E 2259+586 is another source that is associated with an SNR, CTB 109, whose location is assumed to be within or close to the Perseus arm spiral shock at a distance of 3.2 ± 0.2 kpc (R. Kothes & T. Foster 2012). However, for the same source, using red clumps, which are core helium-burning stars and

serve as good infrared standard candles, M. Durant & M. H. van Kerkwijk (2006) estimated the distance as 7.5 \pm 1.0 kpc. Finally, the sources 1E 1841–045 and PSR 1846.4–0258 are associated with SNRs Kesteven 73 and Kesteven 75, whose distances to us were found to be 8.5 $_{-1.0}^{+1.3}$ kpc (W. W. Tian & D. A. Leahy 2008) and 6.0 $_{-0.9}^{+1.5}$ kpc (D. A. Leahy & W. W. Tian 2008a), respectively.

Appendix C Magnetic Field

We present magnetars' burst energies versus their inferred dipolar magnetic field strengths in Figure 5. Note again that for the activities observed with CGRO-BATSE and INTEGRAL from the sources SGR 1900+14 (gold), SGR 1806-20 (green), and SGR 1627-41 (brown), we present burst energy ranges. For details of the observations and the calibration of burst energetics, see Section 2.

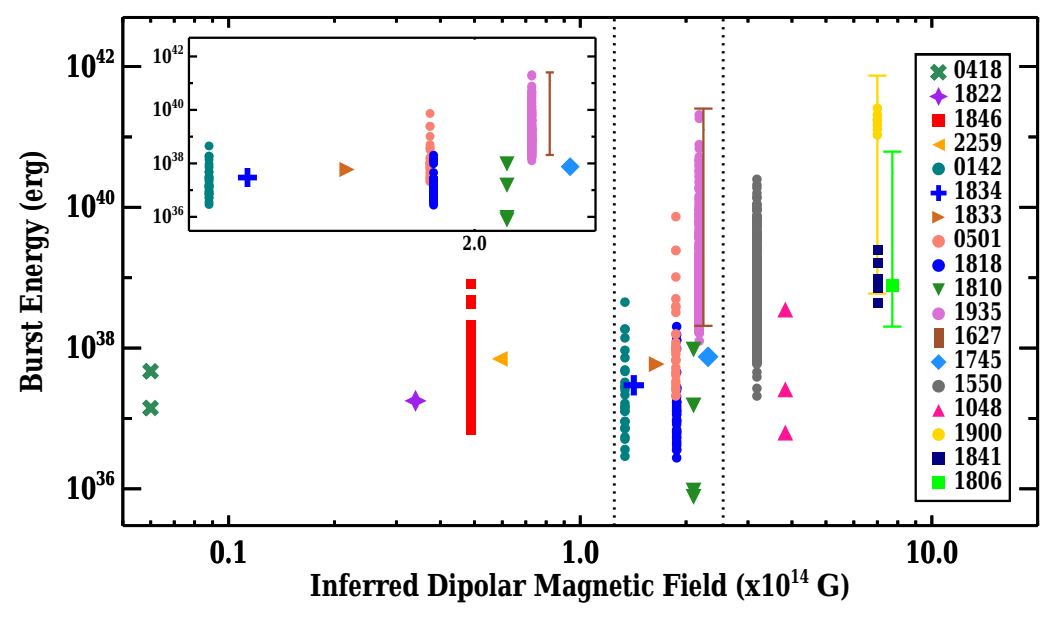


Figure 5. Plot of burst energies vs. inferred dipolar magnetic field strengths of burst-active magnetars. Filled symbols represent the energetics of individual bursts from the color-coded magnetars. For SGR 1900+14 (gold), SGR 1806-20 (green), and SGR 1627-41 (brown), we present burst energy ranges rather than individual burst energies (see text for details). Symbols on the right are ordered in increasing inferred dipolar magnetic field strength. The inset zooms in on the region that remains between the dotted lines.

ORCID iDs

References

```
Aguilera, D. N., Pons, J. A., & Miralles, J. A. 2008, A&A, 486, 255
Ascenzi, S., Viganò, D., Dehman, C., et al. 2024, MNRAS, 533, 201
Baiko, D. A., & Chugunov, A. I. 2018, MNRAS, 480, 5511
Baiko, D. A., & Kozhberov, A. A. 2017, MNRAS, 470, 517
Beloborodov, A. M., & Thompson, C. 2007, ApJ, 657, 967
Bibby, J. L., Crowther, P. A., Furness, J. P., & Clark, J. S. 2008, MNRAS,
  386, L23
Bower, G. C., Deller, A., Demorest, P., et al. 2014, ApJL, 780, L2
Camero, A., Papitto, A., Rea, N., et al. 2014, MNRAS, 438, 3291
Camilo, F., Cognard, I., Ransom, S. M., et al. 2007, ApJ, 663, 497
Cheng, B., Epstein, R. I., Guyer, R. A., & Young, A. C. 1996, Natur, 382, 518
Chugunov, A. I., & Horowitz, C. J. 2010, MNRAS, 407, L54
Collazzi, A. C., Kouveliotou, C., van der Horst, A. J., et al. 2015, ApJS,
Corbel, S., Chapuis, C., Dame, T. M., & Durouchoux, P. 1999, ApJL,
   526, L29
Coti Zelati, F., Rea, N., Pons, J. A., Campana, S., & Esposito, P. 2018,
   MNRAS, 474, 961
Davies, B., Figer, D. F., Kudritzki, R.-P., et al. 2009, ApJ, 707, 844
De Grandis, D., Taverna, R., Turolla, R., et al. 2021, ApJ, 914, 118
Dehman, C., Viganò, D., Ascenzi, S., Pons, J. A., & Rea, N. 2023, MNRAS,
D'Elia, V., Barthelmy, S. D., Baumgartner, W. H., et al. 2011, GCN, 12253, 1
Dib, R., & Kaspi, V. M. 2014, ApJ, 784, 37
Dib, R., Kaspi, V. M., Scholz, P., & Gavriil, F. P. 2012, ApJ, 748, 3
Duncan, R. C., & Thompson, C. 1992, ApJL, 392, L9
Durant, M., & van Kerkwijk, M. H. 2006, ApJ, 650, 1070
Esposito, P., Burgay, M., Possenti, A., et al. 2009a, MNRAS, 399, L44
Esposito, P., Israel, G. L., Turolla, R., et al. 2011, MNRAS, 416, 205
Esposito, P., Tiengo, A., Mereghetti, S., et al. 2009b, ApJL, 690, L105
Gavriil, F. P., Kaspi, V. M., & Woods, P. M. 2002, Natur, 419, 142
Gavriil, F. P., Kaspi, V. M., & Woods, P. M. 2006, ApJ, 641, 418
Gelfand, J. D., & Gaensler, B. M. 2007, ApJ, 667, 1111
Göğüş, E., Cusumano, G., Levan, A. J., et al. 2010, ApJ, 718, 331
Göğüş, E., Kouveliotou, C., Woods, P. M., et al. 2001, ApJ, 558, 228
Göğüş, E., Lin, L., Roberts, O. J., et al. 2017, ApJ, 835, 68
Göğüş, E., Woods, P. M., Kouveliotou, C., et al. 1999, ApJL, 526, L93
Göğüş, E., Woods, P. M., Kouveliotou, C., et al. 2000, ApJL, 532, L121
Gotthelf, E. V., Vasisht, G., Boylan-Kolchin, M., & Torii, K. 2000, ApJL,
  542, L37
Götz, D., Mereghetti, S., Molkov, S., et al. 2006, A&A, 445, 313
Gourgouliatos, K. N., & Lander, S. K. 2021, MNRAS, 506, 3578
Igoshev, A. P., Gourgouliatos, K. N., Hollerbach, R., & Wood, T. S. 2021,
   ApJ, 909, 101
Israel, G. L., Esposito, P., Rea, N., et al. 2016, MNRAS, 457, 3448
Israel, G. L., Romano, P., Mangano, V., et al. 2008, ApJ, 685, 1114
Kaneko, Y., Göğüş, E., Baring, M. G., et al. 2021, ApJL, 916, L7
```

```
Kaneko, Y., Göğüş, E., Kouveliotou, C., et al. 2010, ApJ, 710, 1335
Kargaltsev, O., Kouveliotou, C., Pavlov, G. G., et al. 2012, ApJ, 748, 26
Kaspi, V. M., Archibald, R. F., Bhalerao, V., et al. 2014, ApJ, 786, 84
Kennea, J. A., Burrows, D. N., Kouveliotou, C., et al. 2013, ApJL, 770, L24
Keskin, Ö., Göğüş, E., Kaneko, Y., et al. 2024, ApJ, 965, 130
Kothes, R., & Foster, T. 2012, ApJL, 746, L4
Lander, S. K. 2023, ApJL, 947, L16
Lander, S. K., Gourgouliatos, K. N., Wadiasingh, Z., & Antonopoulou, D.
   2024, arXiv:2411.08020
Leahy, D. A., & Tian, W. W. 2008a, A&A, 480, L25
Leahy, D. A., & Tian, W. W. 2008b, AJ, 135, 167
Lin, L., Göğüş, E., Roberts, O. J., et al. 2020a, ApJ, 893, 156
Lin, L., Göğüş, E., Roberts, O. J., et al. 2020b, ApJL, 902, L43
Lin, L., Kouveliotou, C., Baring, M. G., et al. 2011, ApJ, 739, 87
Livingstone, M. A., Ng, C. Y., Kaspi, V. M., Gavriil, F. P., & Gotthelf, E. V.
  2011, ApJ, 730, 66
Lower, M. E., Shannon, R. M., Johnston, S., & Bailes, M. 2020, ApJL,
  896, L37
Lyutikov, M. 2003, MNRAS, 346, 540
Mereghetti, S., Esposito, P., Tiengo, A., et al. 2006, ApJ, 653, 1423
Minter, A. H., Camilo, F., Ransom, S. M., Halpern, J. P., & Zimmerman, N.
  2008, ApJ, 676, 1189
Mondal, T. 2021, ApJL, 913, L12
Olausen, S. A., & Kaspi, V. M. 2014, ApJS, 212, 6
Perna, R., & Pons, J. A. 2011, ApJL, 727, L51
Pons, J. A., & Geppert, U. 2007, A&A, 470, 303
Rajwade, K. M., Stappers, B. W., Lyne, A. G., et al. 2022, MNRAS, 512, 1687
Rea, N., Israel, G. L., Pons, J. A., et al. 2013, ApJ, 770, 65
Rodríguez Castillo, G. A., Israel, G. L., Tiengo, A., et al. 2016, MNRAS,
  456, 4145
Sánchez-Cruces, M., Rosado, M., Fuentes-Carrera, I., & Ambrocio-Cruz, P.
  2018, MNRAS, 473, 1705
Sasaki, M., Plucinsky, P. P., Gaetz, T. J., & Bocchino, F. 2013, A&A,
Sasaki, M., Plucinsky, P. P., Gaetz, T. J., et al. 2004, ApJ, 617, 322
Scholz, P., Ng, C. Y., Livingstone, M. A., et al. 2012, ApJ, 761, 66
Tendulkar, S. P., Cameron, P. B., & Kulkarni, S. R. 2012, ApJ, 761, 76
Thompson, C., & Duncan, R. C. 1995, MNRAS, 275, 255
Thompson, C., & Duncan, R. C. 2001, ApJ, 561, 980
Thompson, C., Lyutikov, M., & Kulkarni, S. R. 2002, ApJ, 574, 332
Tian, W. W., & Leahy, D. A. 2008, ApJ, 677, 292
Tiengo, A., Vianello, G., Esposito, P., et al. 2010, ApJ, 710, 227
Uzuner, M., Keskin, Ö., Kaneko, Y., et al. 2023, ApJ, 942, 8
van der Horst, A. J., Connaughton, V., Kouveliotou, C., et al. 2010, ApJL,
  711, L1
van der Horst, A. J., Kouveliotou, C., Gorgone, N. M., et al. 2012, ApJ,
  749, 122
Woods, P. M., Kouveliotou, C., Finger, M. H., et al. 2007, ApJ, 654, 470
Woods, P. M., Kouveliotou, C., Finger, M. H., et al. 2000, ApJL, 535, L55
Woods, P. M., Kouveliotou, C., Gavriil, F. P., et al. 2005, ApJ, 629, 985
Woods, P. M., Kouveliotou, C., van Paradijs, J., et al. 1999, ApJL, 519, L139
Xu, Y., Reid, M. J., Zheng, X. W., & Menten, K. M. 2006, Sci, 311, 54
Younes, G., Baring, M. G., & Kouveliotou, C. 2017, ApJ, 851, 17
Younes, G., Kouveliotou, C., & Kaspi, V. M. 2015, ApJ, 809, 165
```